

Article

Not peer-reviewed version

---

# Is Animal Magnetoreception Quantum? A Perspective from the Energy Resolution Limit

---

[Iannis Kominis](#)<sup>\*</sup> and Efthimis Gkoudinakis

Posted Date: 27 September 2024

doi: 10.20944/preprints202409.2178.v1

Keywords: magnetoreception; quantum sensing; quantum biology



Preprints.org is a free multidiscipline platform providing preprint service that is dedicated to making early versions of research outputs permanently available and citable. Preprints posted at Preprints.org appear in Web of Science, Crossref, Google Scholar, Scilit, Europe PMC.

Copyright: This is an open access article distributed under the Creative Commons Attribution License which permits unrestricted use, distribution, and reproduction in any medium, provided the original work is properly cited.

## Article

# Is Animal Magnetoreception Quantum? A Perspective from the Energy Resolution Limit

I. K. Kominis \* and E. Gkoudinakis

Department of Physics, University of Crete, Heraklion 70013, Greece

\* Correspondence: ikominis@uoc.gr

**Abstract:** A large number of magnetic sensors, like superconducting quantum interference devices, optical pumping and nitrogen vacancy magnetometers, were shown to satisfy the energy resolution limit. This limit states that the magnetic sensitivity of the sensor, when translated into a product of energy with time, is bounded below by Planck's constant,  $\hbar$ . This bound implies a fundamental limitation as to what can be achieved in magnetic sensing. Here we explore biological magnetometers, in particular three magnetoreception mechanisms thought to underly animals' geomagnetic field sensing: the radical-pair, the magnetite and the MagR mechanism. We address the question of how close these mechanisms approach the energy resolution limit. At the quantitative level, the utility of the energy resolution limit is that it informs the workings of magnetic sensing in model-independent ways, and thus can provide subtle consistency checks for theoretical models and estimated or measured parameter values, particularly needed in complex biological systems. At the qualitative level, the closer the energy resolution is to  $\hbar$ , the more "quantum" is the sensor. This offers an alternative route towards understanding the quantum biology of magnetoreception. It also quantifies the room for improvement, illuminating what Nature has achieved, and stimulating the engineering of biomimetic sensors exceeding Nature's magnetic sensing performance.

**Keywords:** magnetoreception; quantum sensing; quantum biology

## 1. Introduction

Animal magnetoreception is a major and strongly interdisciplinary scientific puzzle [1–9]. Quoting a 2010 paper [10], "...the solution to the magnetoreception mystery will almost certainly come from a fascinating interplay of biology, chemistry and physics". The quote is as valid today as it was in 2010, since science still awaits the full solution to this challenging problem of sensory biology.

Although numerous behavioural experiments have established the ability of many species to sense the geomagnetic field, the mechanisms behind biological magnetic sensing, and their working at the physical, chemical and physiological level, are still being debated. There is evidence that migratory birds [11–15], fruit flies [16–24], butterflies [25–27], turtles [28–30], sharks [31–33], eels [34–38], salmon [39–41], are among the many species having magnetic sensing capabilities, either at the level of a compass for acquiring directional information towards long-distance navigation, or in some form of a magnetic map for positioning, or both. Three mechanisms have so far been prevalent in the discussion of biological magnetoreception, the radical-pair [42–46], the magnetite [47–51], and the induction mechanism [52–55], while a mechanism synthesizing the first two, the MagR protein complex, was relatively recently proposed [56].

Sensing the magnetic field is by all means a physical process. In this respect, biological magnetometers must have quite some common ground with man-made magnetometers, which in recent decades have made spectacular progress towards highly sophisticated devices. Magnetometers largely based on classical physics have been around for several decades [57–59]. However, significant progress in magnetic sensitivity was driven by modern quantum technology [60,61], a major thrust of which is quantum sensing [62] of magnetic fields.

The reason behind this progress is that at the quantum level, measuring a magnetic field is equivalent to measuring energy. The precision of energy measurements depends on the lifetime of "quantumness", which reflects how well a "fragile" quantum system is isolated from its perturbing environment. Modern quantum experiments have pushed this isolation to new extremes, thus leading

to sensitive magnetic sensing technologies. Among those are superconducting quantum interference devices [63–65], optical pumping magnetometers [66,67], diamond sensors [68–70], Bose-Einstein condensates [71–73].

A major goal of magnetometry is to understand how the physical principles underlying each technology limit the magnetic sensitivity and other figures of merit of the sensor. Quantum physics indeed puts stringent limits to what can be achieved with any kind of sensor, although many times it is challenging to precisely define those limits. Nevertheless, it is broadly accepted that such fundamental measurement limits do exist, and research towards understanding and utilizing them to design new magnetic sensing applications is overly active [74–84].

Recently, another approach gave a more holistic and *technology-independent* perspective on magnetic sensing based on the so-called energy resolution limit (ERL) [85]. The energy resolution (ER), more precisely called energy resolution per bandwidth, is a quantity composed of the uncertainty in the magnetic field estimate performed by the sensor, the sensitive volume, and the measurement time. This quantity has unit of [energy][time], which is the same unit as Planck's constant,  $\hbar$ . It turns out [85] that numerous magnetic sensing realizations spanning many different technologies have energy resolution larger than  $\hbar$ .

Here we use the ERL as a guiding principle for understanding biological magnetoreception using just three basic quantities: sensitivity  $\delta B$ , volume  $V$ , and measurement time  $\tau$ . Biological magnetic sensors should also satisfy the ERL, because after all, biological systems operate under the laws of physics [86]. The ERL can offer multiple insights into animal magnetoreception.

Qualitatively, the closer to  $\hbar$  the numerical value of the ER is for any given sensor, the more “quantum” can the sensor be characterized. This offers an alternative perspective in the study of quantum biology of magnetoreception [87–96]. This discussion is not about a choice between “black” or “white”, since “quantumness” can now be quantified, and spans a continuum. Indeed, there are now quantifiers for quantum coherence [97] and entanglement [98], and some have been applied to quantifying “quantumness” of biological magnetoreception [99,100]. The ER provides yet another quantifier, this time in units of  $\hbar$ . For example, if it is found that some biological magnetic sensor has ER e.g.  $10^7 \hbar$ , and thus is far from the quantum limit, this finding is still quite informative, since it implies room for  $10^7$  improvement. Even if Nature did not have the chance to realize such an improvement, it could in principle be engineered with biomimetic sensors [101–103].

Quantitatively, the ERL provides a strong and subtle constraint of basic and measurable parameters ( $\delta B$ ,  $V$ ,  $\tau$ ). This constraint is particularly helpful for understanding biological magnetoreceptors, which unavoidably face the complexities and uncertainties of biological systems, as opposed to precisely controlled quantum magnetometers in the laboratory. As will be outlined in the paper, some biological ERs do not have a specific value as man-made sensors do, but rather, a range of possible values, stemming from those uncertainties. *Conversely, it will be seen that the ERL narrows down those uncertainties.* For example, we here obtain a precise lower bound for the number of cryptochromes that are required for obtaining a given magnetic sensitivity within a given measurement time.

The outline of this paper is the following. In Sec. II we make some introductory comments about the energy resolution limit aimed at an interdisciplinary readership. We then apply the ERL to the radical-pair (Sec. III), the magnetite (Sec. IV) and the MagR mechanism (Sec. V). In Sec. VI we present the results in a global ERL map. We conclude in Sec. VII.

## 2. Introductory Comments about the Energy Resolution Limit

The authors in [85] analyzed the magnetometry literature and observed that tens of different realizations of several magnetic sensing technologies satisfy a bound, which reads

$$\text{ER} \equiv \frac{(\delta B)^2}{2\mu_0} V \tau \gtrsim \hbar \quad (1)$$

The left-hand-side defines the energy resolution of the sensor, and the right-hand side is Planck's constant  $\hbar = 10^{-34}$  Js, which constant pervades quantum phenomena.

In the expression of the energy resolution,  $\delta B$  is the uncertainty in the sensor's magnetic field estimate,  $V$  the sensitive volume, and  $\tau$  the measurement time. The constant  $\mu_0 = 4\pi \times 10^{-7}$  Tm/A is the magnetic permeability of vacuum. The name "energy resolution" derives from the following. From classical electromagnetism we know that  $B^2/2\mu_0$  is the magnetic energy density (unit J/m<sup>3</sup>) due to the presence of a magnetic field  $B$  in space. For a homogeneous magnetic field, the total energy within some volume  $V$  is then  $B^2V/2\mu_0$ . The ERL involves the variance  $(\delta B)^2$  instead of  $B^2$ , therefore one can loosely think of it as the minimum magnetic energy measurable within the sensor volume during the time available for the measurement. The right-hand-side of (1) is approximately equal to  $\hbar$ , thus it is tempting to guess that some basic quantum principle underlies the ERL.

Here we will not address the intricacies of the quantum physics of the ERL, but for completeness we note that (i) such a principle was recently proposed to derive from quantum thermodynamics [104], and (ii) there are claims for magnetic sensors having an ER below  $\hbar$  [105–107]. Our understanding [104] is that such claims involve non-trivial quantum enhancements that one would hardly expect to find in biological systems, even in light of quantum biological effects [108]. Given that a vast number of technologies do satisfy the ERL [85], we here work under the premise that the same is the case for biological magnetometers.

In Figure 1 we reproduce the results of [85]. The  $y$ -axis displays the quantity  $\widetilde{\delta B} = \delta B\sqrt{\tau}$  (having unit T/ $\sqrt{\text{Hz}}$ ) versus the linear dimension  $L$  of the sensor. This is connected to the volume entering (1) by  $V = L^3$ . The spectral magnetic sensitivity  $\widetilde{\delta B}$  describes how the measurement noise is distributed over the measurement bandwidth, given by  $1/\tau$ . The utility of  $\widetilde{\delta B}$  is that we can produce a common figure for  $\widetilde{\delta B}$  versus  $L$  for a number of sensors having different measurement times  $\tau$ . It is seen in Fig. 1 that all sensors examined have  $\widetilde{\delta B} \geq \sqrt{2\mu_0\hbar/L^3}$ , which is another way to express the bound (1).

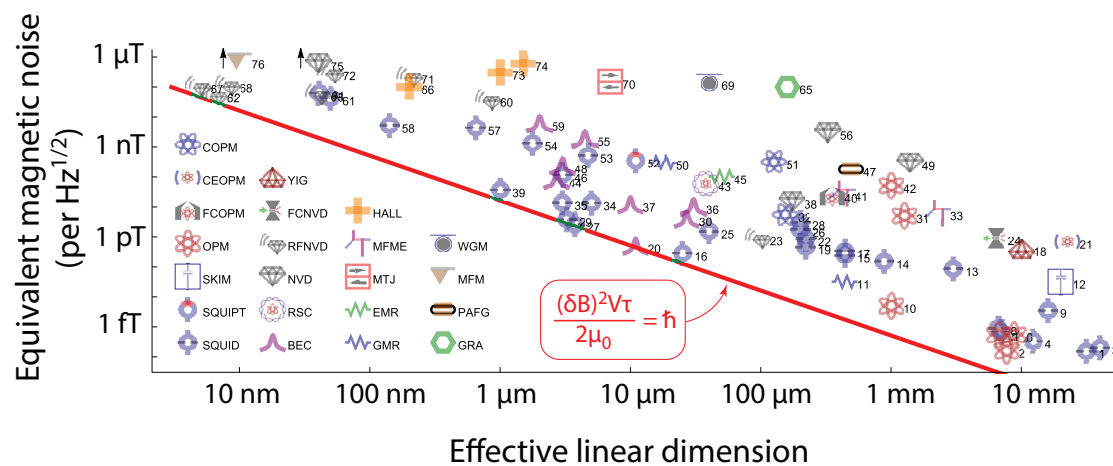


**Figure 1.** Magnetic sensing energy resolution limit [85]. Magnetic sensitivity versus sensor's linear dimension for tens of magnetic sensing realizations of several magnetometers, like atomic magnetometers, SQUIDS, diamond and Hall effects sensors, and more. The red solid line is defined by the energy resolution limit, that is, the bound  $(\delta B)^2V\tau/2\mu_0 \geq \hbar$ , where  $\widetilde{\delta B}$  is the magnetic sensitivity (or equivalently magnetic noise) in units of T/ $\sqrt{\text{Hz}}$ ,  $V$  is the volume of the sensor (the third power of the linear dimension), and  $\mu_0$  vacuum's magnetic permeability constant. If the measurement time is  $\tau$ , and the error in the magnetic field estimate obtained within the measurement time is  $\delta B$ , then  $\widetilde{\delta B} = \delta B\sqrt{\tau}$ . Figure reproduced from [85] with permission of the American Physical Society.

In the next three sections we analyze the energy resolution for the radical-pair, the magnetite, and the MagR mechanism. In the beginning of each section we briefly recapitulate the workings of the relevant mechanism. To establish the ER, we extract from the literature the magnetic sensitivity  $\delta B$ , the

sensor volume  $V$ , and the measurement time  $\tau$ . At the end, we produce a similar map of the global results like the one in Fig. 1.

### 3. Radical-Pair Mechanism

The radical-pair mechanism can provide both a scalar measurement of the magnetic field amplitude, usually referred to as the “magnetic field effect” [109–113], as well as directional information. The former might be used in a magnetic map [6], while the latter in a compass [114–117]. The experimental evidence supporting radical-pair magnetoreception, reviewed e.g. in [6], involves disorientation by radiofrequency magnetic fields, localization in the retina of cryptochrome proteins hosting the radical pairs, and co-localization of cryptochrome with neuronal activity markers [118–125].

Within the perspective of the ERL we focus on the magnetic field amplitude. This does not limit the utility of our results, since as stated in [6], “map and compass cues might not always be as separable as previously thought”. Information on the magnetic field change is reflected in the change in concentration of radical-pair reaction products. We remind the reader that such reactions involve a coherent spin motion, which is influenced by the magnetic field. This spin motion is driven by the intra-molecular magnetic fields produced by the hyperfine couplings of the two unpaired electrons of the donor and acceptor molecule forming the radical-pair with the magnetic nuclei of the respective molecule. The radical-pair is created by photo-excitation of the neutral precursor. The mechanism is depicted in Figure 2a, which shows the photo-excitation step of the donor-acceptor molecular dyad, DA, the electron transfer creating the radical-pair state  $D^{\bullet+}A^{\bullet-}$  in the singlet state of the two unpaired electrons, the coherent spin motion  $^S D^{\bullet+}A^{\bullet-} \leftrightarrow ^T D^{\bullet+}A^{\bullet-}$  interchanging singlet with triplet radical-pair states, and the inverse electron transfer leading to the singlet (DA) and triplet ( $^T$ DA) reaction products.



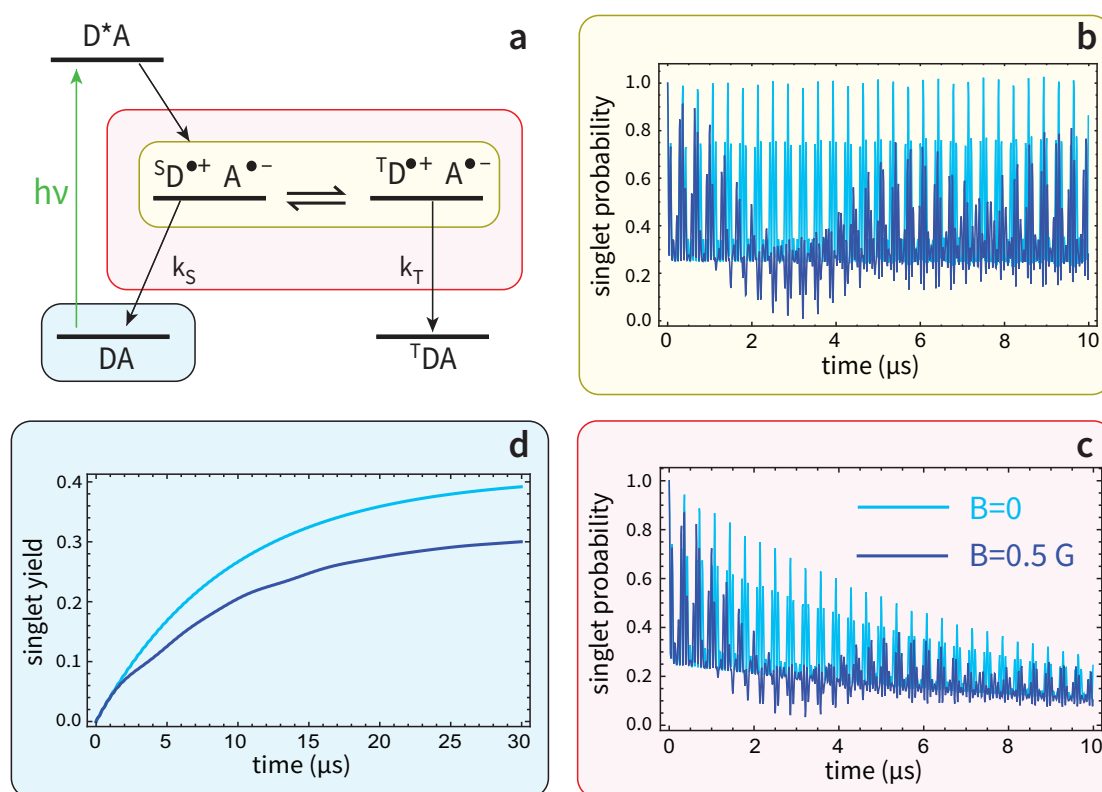


**Figure 2.** Radical-pair mechanism and example of spin dynamics. (a) A donor-acceptor dyad, DA, is photo-excited. The photo-excited state  $D^*A$ , leads by electron transfer to the singlet radical-pair,  $S_D^{\bullet+} A^{\bullet-}$ . Intra-molecule magnetic interactions, including the Zeeman interaction of the two unpaired electrons with the external magnetic field, drive singlet-triplet oscillations, i.e. a coherent interconversion  $S_D^{\bullet+} A^{\bullet-} \leftrightarrow T_D^{\bullet+} A^{\bullet-}$ . The inverse electron transfer from A back to D leads to the neutral recombination products through two recombination channels, the singlet (rate  $k_S$ ) producing DA, and the triplet (rate  $k_T$ ) producing  $T^*DA$ . (b) Example of singlet-triplet oscillations with no recombination, for two different magnetic fields,  $B = 0$  and  $B = 0.5$  G. The y-axis is the singlet probability, given by  $\text{Tr}\{\hat{\rho}_t Q_S\}$ , where  $\hat{\rho}_t$  is the radical-pair spin density matrix at time  $t$ , and  $Q_S$  the singlet projection operator. The model considered here is a radical-pair with two spin-1/2 nuclei, one at D and one at A, the density matrix in this case having dimension 16. The Hamiltonian driving the spin motion is  $\mathcal{H} = B(s_{Dz} + s_{Az}) + a_D \mathbf{s}_D \cdot \mathbf{I}_D + a_A \mathbf{s}_A \cdot \mathbf{I}_A$ , where  $\mathbf{s}_D$  and  $\mathbf{s}_A$  are the electron spins of D and A,  $\mathbf{I}_D$  and  $\mathbf{I}_A$  the nuclear spins of D and A, and  $a_D$  and  $a_A$  the respective hyperfine couplings, here considered isotropic. The dynamics are described by the unitary evolution  $d\rho/dt = -i[\mathcal{H}, \rho]$ . (c) When the recombination channels are taken into account, the singlet probability decays, since population leaves the radical-pairs (i.e.  $\text{Tr}\{\hat{\rho}\}$  decreases) and grows in the neutral products, DA and  $T^*DA$ . The dynamics are now described by a master equation  $d\rho/dt = -i[\mathcal{H}, \rho] - k(Q_S \rho + \rho Q_S - 2Q_S \rho Q_S) - k\rho$ , where the second term produces singlet-triplet dephasing, and the third term accounts for recombination with  $k_S = k_T = k$ . The lifetime of the reaction is defined as  $\tau = 1/k$ . Here  $\tau = 10 \mu\text{s}$ ,  $a_D = 10$  G,  $a_A = 1$  G. (d) The singlet yield as a function of time, given by  $\int_0^t k dt' \text{Tr}\{\hat{\rho}_{t'} Q_S\}$ , is seen to grow with time as more and more radical-pairs recombine. The final yield, obtained for  $t \gg \tau$ , is a physiological observable seen to depend on  $B$ , and thus it can convey the information on magnetic field changes.

The signalling mechanism conveying the change in reaction yields to higher levels of neurophysiological processing is still not understood [100,126]. Therefore, as magnetic-dependent observable one usually considers one of the two reaction yields, e.g the singlet. This is found by integrating the singlet probability of the radical-pair state times the probability for a singlet recombination, which for a time interval  $dt$  is given by  $k_S dt$ . Similarly, the probability for triplet recombination is  $k_T dt$ . The rates  $k_S$  and

$k_T$  are characteristic parameters of the specific radical-pair considered. In general they are different, however, in many simulations they are taken equal,  $k_S = k_T \equiv k$ . In this case, also considered herein,  $\tau = 1/k$  is the reaction time, which will also serve as the measurement time in our ER considerations.

For completeness, in Figure 2b we depict an example of the coherent spin motion  $^S\text{D}^{\bullet+}\text{A}^{\bullet-} \leftrightarrow ^T\text{D}^{\bullet+}\text{A}^{\bullet-}$  for an infinite radical-pair lifetime, i.e.  $k = 0$ . We plot the singlet probability as a function of time for two different magnetic fields, to show how the field modulates the singlet-triplet mixing. In Figure 2c we “turn on” the recombination channels, so in this case we observe the decay of the singlet probability, since radical-pairs recombine and their population tends to zero, while the population of the reaction products increases. This is shown in Fig. 2d for the singlet reaction yield, which is seen to convey the information on the magnetic field. Indeed, for a change from  $B = 0$  to  $B = 0.5$  G, the singlet reaction yield at the end of the reaction ( $t \gg \tau$ ) changes by 10% (in absolute terms).

### 3.1. Energy Resolution of Synthesized Radical-Pairs Probed with Laser Spectroscopy

The authors in [127] synthesized a radical-pair model using a carotenoid-porphyrin-fullerene triad (CPF). The porphyrin serves as an intermediate cation in the electron-transfer process, whereas the actual radical-pair is  $\text{C}^{\bullet+}\text{PF}^{\bullet-}$ , i.e. the carotenoid is the radical cation, and the fullerene is the radical anion. The authors observed a clear magnetic field effect in the radical-pair reaction at earth’s magnetic field, albeit at 113 K, i.e. much cooler than the physiological animal temperature. Nevertheless, these data are perfectly suitable to apply the ERL. The authors measured the transient absorption of the radical-pair state at 39 °T and 49 °T. From the noise in their data (Fig. 2c of [127]) one can estimate the magnetic sensitivity to be  $\delta B \approx 2.5$  °T. The measurement time was  $\tau \approx 1$  ns, given by the duration of the magnetic-field effect. Finally, the sensing volume of the 100 nM CPF solution that was probed by the laser measuring the transient absorption of  $\text{C}^{\bullet+}\text{PF}^{\bullet-}$  was  $V \approx 2 \times 10^{-8} \text{ m}^3$  [128]. Thus in this case, it is  $\text{ER} = (\delta B)^2 V \tau / 2\mu_0 = 5 \times 10^{14} \hbar$ .

The main reason for the large value of this ER is the large value of  $\delta B$  deriving from the specific measurement scheme. It is known from quantum magnetometers working with atomic vapors [129] that the number of atoms participating in the measurement is crucial. The number density of CPF molecules, given their 100 nM concentration, is  $6 \times 10^{16} \text{ cm}^{-3}$ , two orders of magnitude higher than the atom number density of typical optical pumping magnetometers [129], which deliver magnetic sensitivity at the level of 1 fT. Thus,  $\delta B$  is not limited by the number of CPF molecules. Similarly, atomic magnetometers have about 3-4 orders of magnitude longer relaxation time, so again,  $\tau$  is not the limiting factor here. Instead, it appears that the ER is dominated by the limited sensitivity of the specific measurement scheme.

Indeed, the magnetic field effect is measured by detecting an optical absorption exciting the radical-pair state into higher electronically excited states, without any discrimination between singlet or triplet radical-pairs. That is, the magnetic field effect probes the total population of the radical-pair state, given by  $\text{Tr}\{\rho\}$ , where  $\rho$  is the radical-pair density matrix. It can be seen from the master equation evolving  $\rho$  (see caption of Fig. 2) that when calculating  $d\text{Tr}\{\rho\}/dt$ , the Hamiltonian term that contains the magnetic field drops out. When the recombination rates are equal, as in the example of Figure 2, it is  $d\text{Tr}\{\rho\}/dt = -k\text{Tr}\{\rho\}$ , and the sensitivity of  $\text{Tr}\{\rho\}$  to the magnetic field is identically zero. The authors in [127] observed a magnetic field effect because for  $\text{C}^{\bullet+}\text{PF}^{\bullet-}$  it is  $k_S \neq k_T$ , and the reaction terms for unequal recombination rates indirectly produce a magnetic-field dependence of  $\text{Tr}\{\rho\}$ . Still, the magnetic sensitivity when measuring  $\text{Tr}\{\rho\}$  is quite lower than detecting e.g. the singlet product yield, as magnetoreceptive organisms are supposed to do physiologically. Additionally, molecular excitation is not as sharp as the laser probing of atoms, hence the measurement noise appears to be significant.

Overall, the specific ER over-satisfies the ERL bound. The values for  $\widetilde{\delta B} = \delta B \sqrt{\tau}$  and the spatial dimension  $L$  that we will use for CPF magnetoreception in our global results of Sec. VII are  $\widetilde{\delta B} \approx 2.5 \text{ nT}/\sqrt{\text{Hz}}$  and  $L \approx 3 \text{ mm}$ .

### 3.2. What Is $\delta B$ In Vivo?

For the rest of the discussion in this and the following sections, which has to do with animal magnetoreception, we will use a common value for the magnetic sensitivity  $\delta B$ , which we will now infer from the literature. Then, in each of the subsequent models we will additionally obtain the measurement time  $\tau$  and the sensitive volume  $V$  in order to arrive at the corresponding ER.

Several studies of the radical-pair mechanism involve the compass operation resulting from anisotropic hyperfine couplings in the radical-pair [130–132], and leading to  $\phi$ -dependent reaction yields, where  $\phi$  is the angle between the magnetic field and some particular axis defined by a hyperfine tensor. Here we do not consider the compass operation, but the estimate of the magnetic field amplitude. For an order-of-magnitude estimate with a hand-waving approach, we could argue that if the mechanism working as a compass has angular precision  $\delta\phi$ , then one could expect a magnetic field sensitivity  $\delta B \approx B\delta\phi$ , where  $B$  is the background field. On average, the geomagnetic field amplitude is  $B \approx 45 \text{ } \mu\text{T}$ . The angular precision of the compass has been estimated [46,133] as  $\delta\phi \approx 1^\circ$ . Thus  $\delta B \approx 0.8 \text{ } \mu\text{T}$ .

From another perspective, it is known from tracking migratory birds that the position accuracy of homing attributed to long-range navigational cues is around 50 km [6,134]. The magnitude of the geomagnetic field changes by about 3 nT/km in the north-south direction [6], thus over 50 km the change will be  $\delta B \approx 0.15 \text{ } \mu\text{T}$ .

The authors in [135] mention that magnetic anomalies of earth's field, known to be mostly at the level of 1%, could offer navigational cues. This argument would imply  $\delta B = 0.45 \text{ } \mu\text{T}$ . Finally, the authors in [136] use electrophysiological recordings in the trigeminal system of birds and find a  $0.2 \text{ } \mu\text{T}$  sensitivity, while the authors in [137] suggest sensitivities down to the 20 nT level.

The aforementioned numbers involve numerous observations with multiple species, therefore it is virtually impossible to add an error bar weighting the above estimates. Hence we here use the average of all of the above estimates and set  $\delta B = 0.3 \text{ } \mu\text{T}$ .

### 3.3. Energy Resolution In Vivo: Cryptochrome

A prevalent model [138–151] for radical-pair based magnetoreception has been the radical-pair reaction following electron transfer from a triad of tryptophan residues (Tr) to flavin adenine dinucleotide (FAD), with the radical-pair  $\text{FAD}^{\bullet-}\text{Tr}^{\bullet+}$  embedded in the protein cryptochrome (Cry), in particular Cry4. This protein is expressed in the retina of the European robin and exhibits strong binding with flavin [6,152–154]. Recently a tetrad of tryptophans was considered [147], and we will here use this model, depicted in Figure 3. In the same figure we depict the known distances between the radicals, from which we can estimate the volume of the sensor as  $V = 2.1 \text{ nm} \times (0.8 \text{ nm})^2 = 1.4 \times 10^{-27} \text{ m}^3$ .



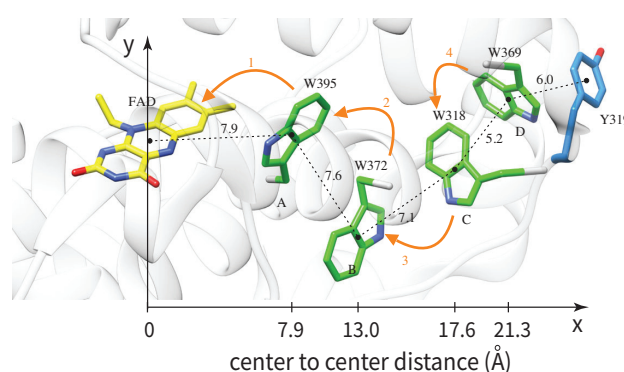


**Figure 3.** Cryptochrome protein (shaded grey background) is the host of the  $\text{FAD}^{\bullet-}\text{Tr}^{\bullet+}$  radical-pair working as a magnetic sensor. Center-to-center distances between FAD and tryptophans are known and provide the overall volume of the sensor. We estimate the length of the sensor from the FAD-W369 distance (21.3 ) and the width from the W372-W369 distance projected on the  $y$ -axis (8 ). Figure reproduced from [147] under the Creative Commons Attribution License.

Lastly, we need to estimate the measurement time  $\tau$ , given by the lifetime of the  $\text{FAD}^{\bullet-}\text{Tr}^{\bullet+}$  radical-pair. The lifetime of  $\text{FAD}^{\bullet-}\text{Tr}^{\bullet+}$  in vivo is not yet known. In vitro measurements at 1 °C report 6  $\mu\text{s}$  [155,156]. As suggested in [157], a lower bound on  $\tau$  is given by the electron spin precession time in earth's field, which is 0.7  $\mu\text{s}$ . The authors in [158] find an operational window of the compass for  $\tau = 10 \mu\text{s}$ , given the relaxation produced by rotational motion of the radical-pair, in particular FAD, and taking into account the sharp “needle” described in [46]. The latter is an impressively sharp feature appearing in the angular dependence of the reaction yields for lifetimes larger than  $\tau = 5 \mu\text{s}$ , when the realistic hyperfine tensors for  $\text{FAD}^{\bullet-}\text{Tr}^{\bullet+}$  are used. If we allow ourselves to hypothesize, it seems unlikely that Nature did not evolve to take advantage of this feature. Based on all of the above, we here set  $\tau = 10 \mu\text{s}$ .

Putting it altogether, it follows that  $\text{ER} = 4.8 \times 10^{-6}\hbar$ . Is the ERL violated? Not at all. The previous result shows that the signal from at least  $N_{\text{cry}}^0 = 1/(4.8 \times 10^{-6}) \approx 2 \times 10^5$  cryptochrome proteins must be physiologically integrated in order to obtain the magnetic sensitivity  $\delta B$  within the time  $\tau$ . *This is exactly the utility of the ERL, it informs the workings of this magnetoreception mechanism in model-independent ways.* If, for example, it is found that indeed there are only  $N_{\text{cry}}^0$  proteins contributing, then cryptochrome magnetoreception will be working right at the quantum limit. On the other hand, it is found that there are e.g. ten times as many proteins contributing, then cryptochrome magnetoreception will be working at the level of  $10\hbar$ , and there is in principle room for a ten-fold improvement, were one to mimic Nature.

Overall, the values for  $\widetilde{\delta B} = \delta B\sqrt{\tau}$  and the spatial dimension  $L$  that we will use for cryptochrome magnetoreception in our global results of Sec. VII are  $\widetilde{\delta B} \approx 1 \text{ nT}/\sqrt{\text{Hz}}$  and  $L = (N_{\text{cry}}V)^{1/3} \geq 66 \text{ nm}$ , where  $N_{\text{cry}}$  the number of cryptochrome proteins contributing to the estimate of the magnetic field, and necessarily, it is  $N_{\text{cry}} \geq N_{\text{cry}}^0$ .

### 3.4. Comment on the Sensor Volume

One might rightly wonder why in the discussion of CPF in Sec. III.A we considered the whole volume of the solution probed by the laser, whereas in the discussion of cryptochrome in Sec. III.C we counted individual sensors, i.e. we multiplied the volume of the  $\text{FAD}^{\bullet-}\text{Tr}^{\bullet+}$  sensor with the number of such sensors, which is the number of cryptochrome proteins involved in magnetoreception. An analogy with optical pumping magnetometers [129] will facilitate this discussion.

Such magnetometers, schematically shown in Figure 4a, involve atomic spins in the vapor phase, with the atomic vapor enclosed in a glass cell. The atoms' spin state, conveying information about the magnetic field, is probed by a laser. One can use a photodiode detecting the whole laser beam,

alternatively, one can use a photodiode array (Figure 4b). The array consists of  $n$  photosensitive elements. If one detects the individual signals  $s_1, s_2, \dots, s_n$ , then each signal conveys information about the magnetic field experienced by the atoms inside the volume defined by the area of one element and the laser path length through the vapor (Figure 4c). If, on the other hand, the  $n$  individual signals are integrated (Figure 4d), information about the magnetic field within the aforementioned elementary volumes is lost, and the sensitive volume is now defined by the laser path length in the vapor and the whole area of the photodiode array (essentially, this is the total vapor volume, when the laser beam waist covers the whole cell).

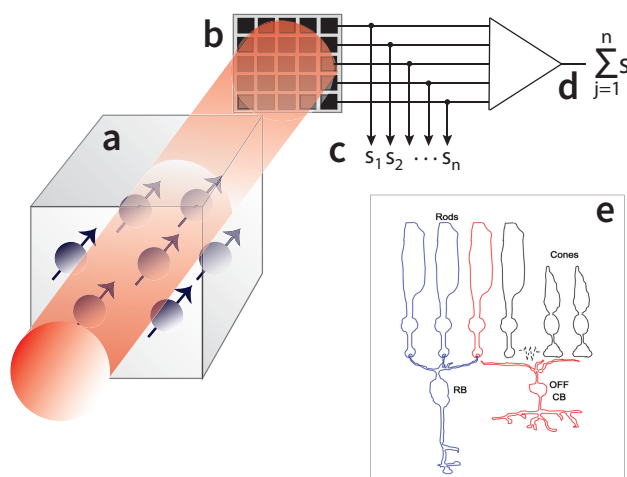


**Figure 4.** (a) Sensitive volume in atomic vapor magnetometers. An ensemble of spins in an atomic vapor is enclosed in a cell and probed by a laser, which is detected by (b) a photodiode array. (c) If one measures the individual signals,  $s_1, s_2, \dots, s_n$ , produced by the array, then the sensitive volume is determined by the area of one photosensitive element and the laser path length in the vapor. (d) If one integrates the  $n$  signals produced by the array, the sensitive volume is determined by the whole area of the photodiode array and the path length, essentially the total volume of the vapor (if the laser waist covers the whole cell). (e) In the retina, rod cells are similarly integrated by bipolar cells (figure reproduced from [159] under the Creative Commons Attribution License).

Biological systems have devised such integration mechanisms. For example (Fig. 4e), rod cells in the retina are integrated by bipolar cells. Going back to magnetoreception, if a number of magnetoreceptive elements are integrated and thus contribute as a whole to the biochemical signal conveying a magnetic field change ( $B \rightarrow B + \delta B$ ) to the animal's brain, then the sensitive volume is the volume of each element times their number. But then, in atomic sensors why isn't the sensitive volume defined by the atomic volume (about  $10^{-30}$  m<sup>3</sup>) times the number of atoms in the vapor, but instead [85], it is defined by the volume occupied by the whole vapor?

A more fundamental way to address this issue is the following. In the derivation of the ERL presented in [104], it is shown that it is the information flow between "system" and "meter" that plays a crucial role. In quantum measurements, two parties are involved in the measurement process, the "system" e.g. the spin, and another physical object interacting with the system, called the "meter". Due to their interaction, information about the system's state is encoded in the meter. The information flow between system and meter takes place inside the sensitive volume during the measurement time. In atomic vapors the meter is another atom of the vapor itself, with every atom experiencing many collisions with other atoms and exchanging information about each others' spin state, while relaxing the spin. It is thus all kinds of binary collisions within the whole vapor that drive these effects. The probing laser cannot resolve these local effects, hence the sensitive volume is defined by the volume of the whole vapor.

Equivalently, within the spin coherence time one atom in the vapor samples a volume much larger than the atomic volume itself. For example, such vapors usually include a buffer gas to eliminate spin relaxation at the cell walls. Even for buffer gas pressures as large as e.g. 5 atm, the diffusion constant of alkali vapors in e.g. nitrogen is  $D \approx 0.06 \text{ cm}^2/\text{s}$ , thus the atom samples a volume of  $(DT_2)^{3/2} \approx 10^{-22} \text{ m}^3$  within the spin coherence time of about  $T_2 \approx 10 \text{ ms}$ . This volume is 8 orders of magnitude larger than the atomic volume.

In the case of radical-pairs in cryptochrome, it is the reaction products that convey the information on the magnetic field, and these are initially *localized* in the volume defined earlier. The  $\text{FAD}^{\bullet-}\text{Tr}^{\bullet+}$  radical-pair is also localized in its protein host. The reaction products could diffuse elsewhere, and they might trigger many more information transfer processes, but fundamentally, the termination of the measurement is the end of the reaction, taking place within the volume defined by  $\text{FAD}^{\bullet-}\text{Tr}^{\bullet+}$ . Put differently, it is hard to suggest any “non-local” interactions that would affect spin dynamics of one  $\text{FAD}^{\bullet-}\text{Tr}^{\bullet+}$  radical-pair hosted in one cryptochrome, with another pair hosted in another cryptochrome, which is about 10 nm away (the size of cryptochrome, 5 times as large as the size of  $\text{FAD}^{\bullet-}\text{Tr}^{\bullet+}$ ). This is because interactions like exchange or dipolar fade away with distance fast enough [160] to have an appreciable inter-cryptochrome effect.

Even if we consider a free radical at the “outskirts” of cryptochrome, i.e. a distance of 10 nm away from the  $\text{FAD}^{\bullet-}\text{Tr}^{\bullet+}$  pair, the dipolar magnetic field produced would be about 10  $\mu\text{T}$ , comparable to earth’s field, hard to reconcile with a working magnetoreceptor. In a nutshell, the assumption that spin relaxation in  $\text{FAD}^{\bullet-}\text{Tr}^{\bullet+}$  is local seems rather likely. In such case, the magnetoreceptor’s volume is  $N_{\text{cry}}$  times the volume of the radical-pair molecule. Essentially, the total volume scaling as  $N_{\text{cry}}$  means that the magnetic sensitivity  $\delta B$  scales as  $1/\sqrt{N_{\text{cry}}}$ , which is the standard statistical gain over many independent repetitions of a measurement.

In the case of CPF, on the other hand, the typical distance between molecules is 25 nm, while the size of CPF is about 8 nm, and solvation effects in electron-transfer dynamics can make non-local effects more pronounced compared to cryptochrome. The probing laser does not resolve such effects, thus we defined the sensitive volume with the volume of the solution probed by the laser.

#### 4. Magnetite Mechanism

The magnetite mechanism is based on the idea of a small permanent magnet moving like a compass needle due to its interaction with the geomagnetic field [48]. Magnetotactic bacteria use magnetite or greigite particles for navigating in the aquatic environment [161–165]. It was the presence of ferrimagnetic materials in numerous magnetoreceptive animal species [166–171] that inspired the magnetite mechanism [172–174].

Since such materials were located in the upper beak, in particular in the ophthalmic nerve (Figure 5a) of birds [175–178], the general physical process that emerged assumes motion of the magnetic material caused by earth’s field, and detection of this motion by neurophysiological means [179–182].

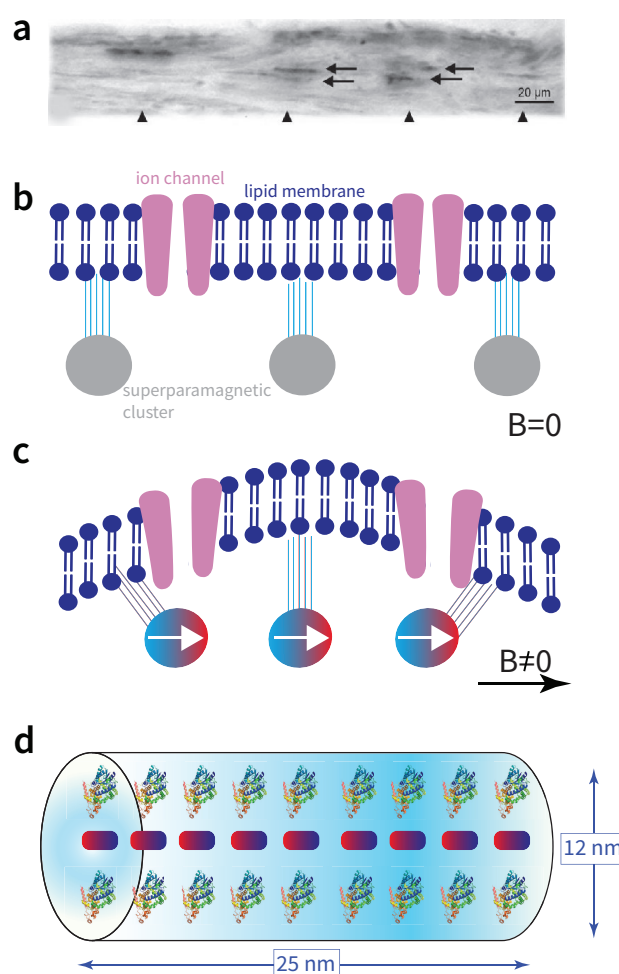


**Figure 5.** (a) Axon bundle with several iron containing dendrites (figure reproduced from [176] under the Creative Commons Attribution License). (b) Magnetoreception model based on a chain of superparamagnetic clusters attached to a membrane [183]. (c) When the magnetic field is non-zero and points along the chain, the clusters get magnetized along the same direction and attract each other, deforming the membrane and conveying the magnetic field change by changing ion-channel currents. If the magnetic field points perpendicular to the chain (not shown here), the clusters repel each other. (d) Geometry of the MagR-cryptochrome protein complex as derived from the measurements presented in [56].

We will here consider a representative such model. The authors in [183] consider superparamagnetic clusters of size  $1\ \mu\text{m}$ , in particular a chain of 20 such clusters separated by about  $1.6\ \mu\text{m}$ . Thus, the volume of the sensor is  $V \approx 20 \times 1.6\ \mu\text{m} \times \pi(0.5\ \mu\text{m})^2 \approx 3 \times 10^{-17}\ \text{m}^3$ . The superparamagnetic particles are supposed to be attached to a neuron's membrane, as shown in Figure 5b depicting the geometry at zero applied field. For a non-zero magnetic field along the chain, the particles are magnetized as shown in Figure 5c, pulling each other and deforming the membrane [184]. This deformation could alter the open/closed probability of ion channels, and thus convey the magnetic field change to the brain via action potentials. The authors estimate a force acting between the clusters of order  $F_m = 10^{-13}\chi^2\ \text{N}$ , where  $\chi$  is the susceptibility of the superparamagnetic material. From relevant measurements [185] it follows that  $\chi \approx 1$ , thus  $F_m \approx 10^{-13}\ \text{N}$ .

To evaluate the measurement time  $\tau$  we neglect the elastic properties of the filaments attaching the clusters to the membrane and consider just two forces acting on the spherical cluster, the magnetic force  $F_m$  and the drag force of the cytoplasm  $F_d$ . The latter is given by  $F_d = 6\pi\eta_c r v$ , where  $\eta_c \approx$

$3.5 \times 10^{-3}$  Ns/m<sup>2</sup> is the cytoplasm viscosity, known to be 5 times that of water [186],  $v$  the sphere's velocity, and  $r$  its radius. The sphere, of mass density about  $\rho_s = 5$  g/cm<sup>3</sup>, reaches its terminal velocity,  $v = F_m/6\pi\eta_c r \approx 3$   $\mu$ m/s, within time  $2\rho_s r^2/9\eta_c \approx 30$  ns.

We now assume that the measurement time is given by the time it takes for the sphere to travel a distance equal to the ion-channel's width of order 1 nm [187]. Using the value of the terminal velocity we find  $\tau \approx 0.3$  ms. In fact, this timescale also reflects the typical frequency of elastic vibrations of the membrane. Indeed, the authors in [188] measure a fundamental flexural frequency of about 10 kHz for a cell having diameter 10  $\mu$ m. If the surface of the deformed membrane considered herein is determined by the length of the chain, i.e.  $32 \mu\text{m} \times 32 \mu\text{m}$ , and considering that the frequency is inversely proportional to the square root of the membrane's mass (and thus its surface area), we find a flexural mode of 5.5 kHz for our case, translating to  $\tau \approx 0.2$  ms. We thus set  $\tau = 0.3$  ms.

Putting it altogether, it follows that  $ER = 3 \times 10^6 \hbar$ . We note that works like [189,190] questioned aspects of magnetite-based magnetoreception. From the perspective of the ERL, the particular mechanism examined here is physically allowed, nevertheless, it should be obvious that the ERL does not prove the mechanism is actually realized as thought at the physiological level. Moreover, the ERL demonstrates that this mechanism requires just one unit of this sensor (i.e. just one chain of superparamagnetic clusters) for obtaining the magnetic sensitivity  $\delta B$  within the time  $\tau$ .

Overall, the values for  $\widetilde{\delta B} = \delta B \sqrt{\tau}$  and the spatial dimension  $L$  that we will use for magnetite magnetoreception in our global results of Sec. VII are  $\widetilde{\delta B} \approx 5$  nT/ $\sqrt{\text{Hz}}$  and  $L = V^{1/3} = 3$   $\mu$ m.

## 5. MagR

The authors in [56,191–194] used genome-wide screening and a tour-de-force experimental validation to discover an iron-sulphur cluster protein, called MagR, which forms a rod-like complex with cryptochromes. The geometry of the rod is shown in Figure 5d. It has a length of 25 nm and diameter of 12 nm, thus volume  $V = 3 \times 10^{-24}$  m<sup>3</sup>. The workings of this complex are not yet understood. It might turn out that the cryptochromes work synergistically with MagR, in some sort of synthesis of the two mechanisms considered previously. We here make this working assumption. Since (i) the biophysics of the MagR complex remains to be unravelled, and (ii) the cryptochrome magnetoreception has a  $\tau$  about one order of magnitude smaller than the  $\tau$  of the magnetite mechanism, we here use as measurement time  $\tau$  the geometric mean of these two numbers, i.e.  $\tau = 80$   $\mu$ s. The resulting ER is  $0.08 \hbar$ , meaning that just  $N_{\text{MagR}}^0 = 1/0.08 = 12$  complexes need to be integrated for the mechanism to hit the ERL bound.

Overall, the values for  $\widetilde{\delta B} = \delta B \sqrt{\tau}$  and the spatial dimension  $L$  that we will use for MagR magnetoreception in our global results of Sec. VII are  $\widetilde{\delta B} \approx 2$  nT/ $\sqrt{\text{Hz}}$  and  $L = (N_{\text{MagR}} V)^{1/3} \geq 33$  nm, where  $N_{\text{MagR}}$  is the number of MagR complexes contributing to the estimate of the magnetic field, and necessarily, it is  $N_{\text{MagR}} \geq N_{\text{MagR}}^0$ .

## 6. Global ER MAP for biological magnetoreception

In Figure 6 we present the global map of the spectral magnetic sensitivity given by  $\widetilde{\delta B} = \delta B \sqrt{\tau}$  as a function of the sensor's linear dimension  $L$  for all sensing mechanisms we have considered. We remind the reader that we used a common value for the magnetic sensitivity,  $\delta B = 0.3$   $\mu$ T. The parameters that differ for each sensing mechanism are the measurement time  $\tau$  and the linear dimension  $L$ . From the global map we can draw a number of conclusions.



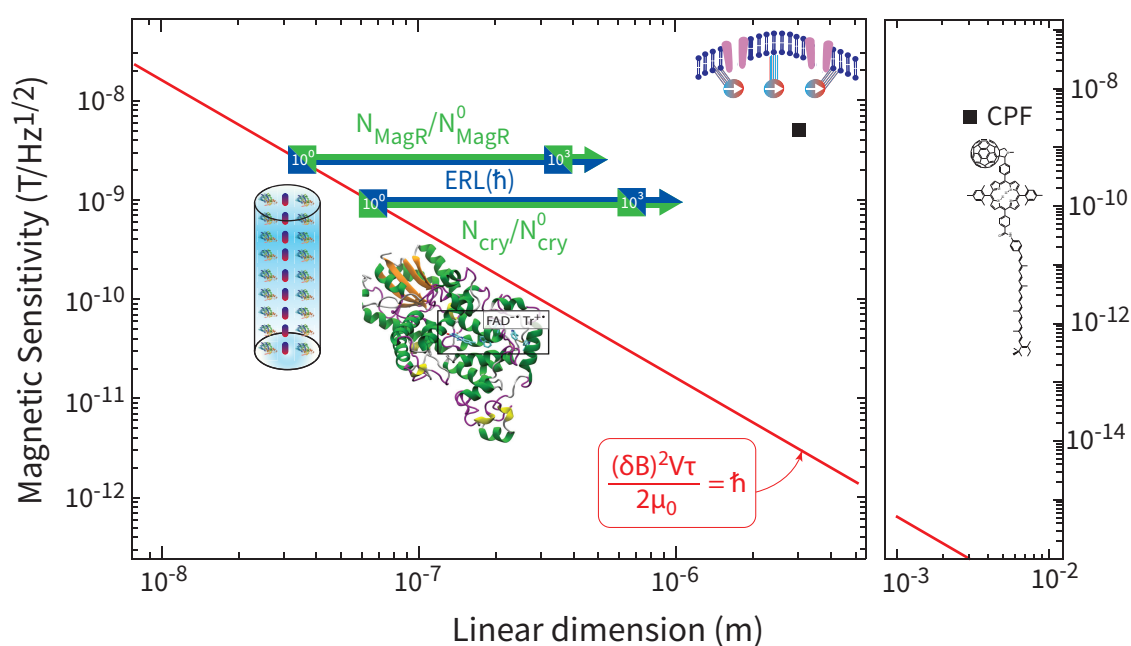


**Figure 6.** Magnetic sensitivity  $\widetilde{\delta B} = \delta B \sqrt{\tau}$  as a function of  $L$ , the linear dimension of the sensor, for several mechanisms considered in animal magnetoreception. The red solid line defines the energy resolution limit given by  $\widetilde{\delta B} = \sqrt{2\mu_0 \hbar / L^3}$ . Cryptochrome magnetoreception based on the FAD-Tr radical-pair sits right at the limit when  $N_{\text{cry}}^0 = 2 \times 10^5$  cryptochromes contribute to a magnetic sensitivity of  $\delta B = 0.3 \mu\text{T}$  within time  $\tau = 10 \mu\text{s}$ . If the number of contributing cryptochromes is e.g.  $10^3$  times larger than  $N_{\text{cry}}^0$ , the total volume of the radical-pair sensor, and thus the ERL, also increases by  $10^3$ , while the linear dimension by 10. This is depicted by the green/blue arrows pointing towards increasing linear dimension. The blue arrow shows the ER in units of  $\hbar$ , and the green arrow the ratio  $N_{\text{cry}}/N_{\text{cry}}^0$ . Similar comments apply to the MagR sensor, shown to hit the ERL when only  $N_{\text{MagR}}^0 = 12$  MagR-protein complexes contribute to detecting the same  $\delta B$  within  $\tau = 80 \mu\text{s}$ . For the magnetite mechanism involving a chain of superparamagnetic clusters it is  $\widetilde{\delta B} = 5 \text{ nT} / \sqrt{\text{Hz}}$  for a linear dimension of  $3 \mu\text{m}$ . The laser spectroscopic measurement of CPF takes place in a solution of  $3 \text{ mm}$  linear dimension, with the corresponding sensitivity being  $\widetilde{\delta B} = 2.5 \text{ nT} / \sqrt{\text{Hz}}$ . Picture of cryptochrome protein adapted from [149] under the Creative Commons Attribution License.

From the perspective of the ERL, the radical-pair magnetoreception can indeed be “quantum”, if the number  $N_{\text{cry}}$  of cryptochromes participating in the sensing is  $N_{\text{cry}} = N_{\text{cry}}^0 = 2 \times 10^5$  (which number depends on the specific values of  $\delta B$  and  $\tau$ ). For  $N_{\text{cry}} > N_{\text{cry}}^0$ , the energy resolution grows beyond  $\hbar$ , and the “quantumness” is reduced. Similar comments apply to the MagR sensor, with the relevant minimum number of contributing complexes being  $N_{\text{MagR}}^0 = 12$ .

The magnetite mechanism, and even more so the CPF measurement appear to be more “classical”, which is probably not surprising. Nevertheless, the ER of the magnetite mechanism stands at the level of  $10^6 \hbar$ , which is not too far from the quantum limit. As interactions of magnetized materials with the magnetic field are at their core quantum, one could imagine pushing the magnetite mechanism closer to the quantum limit with biomimetic engineering.

## 7. Conclusions

Magnetometry is an increasingly active field of quantum technology, with several magnetic sensing technologies competing in terms of sensitivity and applications in fundamental and applied science. The energy resolution is a concept unifying numerous magnetic sensing technologies. Nature has also developed magnetometers, since the geomagnetic field offers a rather stable navigation cue. Here we made the connection between the energy resolution limit, a concept developed by the quantum

sensing community, with biological magnetoreception. We thus arrived at a model-independent consistency check, which informs the workings of several mechanisms aspiring to explain animal magnetoreception. The energy resolution of each magnetoreception mechanism not only provides information about uncertain system parameters, but also illuminates the room for improvement, were one to design a biomimetic sensor. Our considerations thus offer a new perspective on quantum biology, synthesizing quantum sensing with biological sensing, and highlighting the future potential of such synthesis.

In particular, the most obvious utility of the energy resolution limit is to extract information about unknown system parameters. For example, given the magnetic sensitivity and the measurement time of the cryptochrome and MagR magnetoreceptors, we extract for the first time the minimum number of magnetoreceptors required for sensing, since it is this minimum number that is required to satisfy the ERL bound. Conversely, the fact that a given magnetic sensing model might satisfy the ERL, as for example the magnetite model does, is not proof that the model is correct, but merely shows it is a physically viable model.

The results presented here will evolve together with a more precise understanding of the relevant parameters expected from future experiments *in vivo* and *in vitro*. For example, we used a common value for the magnetic sensitivity  $\delta B$  applicable to all magnetoreception mechanisms and animal species. This might be better specified in the future, however the utility of the ERL will be the same, still helping to constrain the sensor's three parameters involving sensitivity, volume and measurement time.

From the quantum engineering perspective, the ERL informs about the extent that a given naturally appearing magnetoreception mechanism can be improved if one develops biomimetic sensors. This work can thus support quantum biotechnology inspired by Nature.

**Acknowledgments:** We kindly acknowledge helpful comments by Kevin Henbest, Peter Hore and Michael Winklhofer.

## References

1. W. T. Keeton, *Magnets interfere with pigeon homing*, Proc. Natl. Acad. Sci. USA **68**, 102 (1971).
2. A. J. Kalmijn, *Biophysics of geomagnetic field detection*, IEEE Trans. Magnetism **17**, 1113 (1981).
3. S. Johnsen and K. J. Lohmann, *The physics and neurobiology of magnetoreception*, Nat. Rev. Neurosci. **6**, 703 (2005).
4. W. Wiltschko and R. Wiltschko, *Magnetic orientation and magnetoreception in birds and other animals*, J. Comp. Physiol. A **191**, 675 (2005).
5. S. Johnsen and K. J. Lohmann, *Magnetoreception in animals*, Phys. Today **61**, 29 (2008).
6. H. Mouritsen, *Long-distance navigation and magnetoreception in migratory animals*, Nature **558**, 50 (2018).
7. J. Xu, L. E. Jarocho, T. Zollitsch, M. Konowalczyk, K. B. Henbest, S. Richert, M. J. Golesworthy, J. Schmidt, V. Déjean, D. J. C. Sowood, M. Bassetto, J. Luo, J. R. Walton, J. Fleming, Y. Wei, T. L. Pitcher, G. Moise, M. Herrmann, H. Yin, H. Wu, R. Bartölke, S. J. Käsehausen, S. Horst, G. Dautaj, P. D. F. Murton, A. S. Gehrckens, Y. Chelliah, J. S. Takahashi, K.-W. Koch, S. Weber, I. A. Solov'yov, C. Xie, S. R. Mackenzie, C. R. Timmel, H. Mouritsen, and P. J. Hore, *Magnetic sensitivity of cryptochrome 4 from a migratory songbird*, Nature **594**, 535 (2021).
8. M. R. Bellinger, J. Wei, U. Hartmann, H. Cadiou, M. Winklhofer, and M. A. Banks, *Conservation of magnetite biomineralization genes in all domains of life and implications for magnetic sensing*, Proc. Natl. Acad. Sci. USA **119**, e2108655119 (2022).
9. C. Xie, *Searching for unity in diversity of animal magnetoreception: from biology to quantum mechanics and back*, Innov. **3**, 100229 (2022).
10. K. J. Lohmann, *Magnetic-field perception*, Nature **464**, 1140 (2010).
11. W. Wiltschko and R. Wiltschko, *Magnetic orientation in birds*, J. Exp. Biol. **199**, 29 (1996).
12. H. Mouritsen and T. Ritz, *Magnetoreception and its use in bird navigation*, Curr. Opin. Neurobiol. **15**, 406 (2005).
13. D. A. Kishkinev and N. S. Chernetsov, *Magnetoreception systems in birds: a review of current research*, Biol. Bull. Rev. **5**, 46 (2015).
14. R. Wiltschko, M. Ahmad, C. Nießner, D. Gehring, and W. Wiltschko, *Light-dependent magnetoreception in birds: the crucial step occurs in the dark*, J. R. Soc. Interface **13**, 20151010 (2016).

15. R. Wiltschko and W. Wiltschko, *Magnetoreception in birds*, J. R. Soc. Interface **16**, 20190295 (2019).
16. J. B. Phillips and O. Sayeed, *Wavelength-dependent effects of light on magnetic compass orientation in *Drosophila melanogaster**, J. Comp. Physiol. **172**, 303 (1993).
17. R. J. Gegear, A. Casselman, S. Waddell, and S. M. Reppert, *Cryptochrome mediates light-dependent magnetosensitivity in *Drosophila**, Nature **454**, 1014 (2008).
18. D. H. Dommer, P. J. Gazzolo, M. S. Painter, J. B. Phillips, *Magnetic compass orientation by larval *Drosophila melanogaster**, J. Insect Phys. **54**, 719 (2008).
19. J.-E. Bae, S. Bang, S. Min, S.-H. Lee, S.-H. Kwon, Y. Lee, Y.-H. Lee, J. Chung and K.-S. Chae, *Positive geotactic behaviors induced by geomagnetic field in *Drosophila**, Molec. Brain **9**, 55 (2016).
20. I.-T. Oh, H.-J. Kwon, S.-C. Kim, H.-J. Kim, K. J. Lohmann, and K.-S. Chae, *Behavioral evidence for geomagnetic imprinting and transgenerational inheritance in fruit flies*, Proc. Natl. Acad. Sci. USA **117**, 1216 (2020).
21. A. Bradlaugh, A. L. Munro, A. R. Jones, and R. A. Baines, *Exploiting the fruitfly, *Drosophila melanogaster*, to identify the molecular basis of cryptochrome-dependent magnetosensitivity*, Quantum Rep. **3**, 127 (2021).
22. A. A. Bradlaugh, G. Fedele, A. L. Munro, C. N. Hansen, J. M. Hares, S. Patel, C. P. Kyriacou, A. R. Jones, E. Rosato, R. A. Baines, *Essential elements of radical pair magnetosensitivity in *Drosophila**, Nature **615**, 111 (2023).
23. M. Bassetto, T. Reichl, D. Kobylkov, D. R. Kattinig, M. Winklhofer, P. J. Hore, and H. Mouritsen, *No evidence for magnetic field effects on the behaviour of *Drosophila**, Nature **620**, 595 (2023).
24. S. M. Reppert, *Magnetic field effects on behaviour in *Drosophila**, Nature **629**, E1 (2024).
25. S. M. Reppert, R. J. Gegear, and C. Merlin, *Navigational mechanisms of migrating monarch butterflies*, Trends Neurosci. **33**, 399 (2010).
26. P. A. Guerra, R. J. Gegear, and S. M. Reppert, *A magnetic compass aids monarch butterfly migration*. Nat. Commun. **5**, 4164 (2014).
27. G. Wan, A. N. Hayden, S. E. Liams, and C. Merlin, *Cryptochrome 1 mediates light-dependent inclination magnetosensing in monarch butterflies*. Nat. Commun. **12**, 771 (2021).
28. V. Courtillot, G. Hulot, M. Alexandrescu, J.-L. le Mouél, and J. L. Kirschvink, *Sensitivity and evolution of sea-turtle magnetoreception: observations, modelling and constraints from geomagnetic secular variation*, Terra Nova, **9**, 203 (1997).
29. K. J. Lohmann, *Sea turtles: navigating with magnetism*, Curr. Biol. **17**, R102 (2007).
30. W. P. Irwin and K. J. Lohmann, *Disruption of magnetic orientation in hatchling loggerhead sea turtles by pulsed magnetic fields*, J. Comp. Physiol. A **191**, 475 (2005).
31. J. M. Anderson, T. M. Clegg, L. V. M. V. Q. Vêras, and K. N. Holland, *Insight into shark magnetic field perception from empirical observations*, Sci. Rep. **7**, 11042 (2017).
32. B. A. Keller, N. F. Putman, R. D. Grubbs, D. S. Portnoy, and T. P. Murphy, *Map-like use of Earth's magnetic field in sharks*, Curr. Biol. **31**, 2881 (2021).
33. C. G. Meyer, K. N. Holland, and Y. P. Papastamatiou, *Sharks can detect changes in the geomagnetic field*, J. R. Soc. Interface **2**, 129 (2005).
34. T. Nishi, G. Kawamura, and K. Matsumoto, *Magnetic sense in the Japanese eel, *Anguilla japonica*, as determined by conditioning and electrocardiography*, J. Exp. Biol. **207**, 2965 (2004).
35. C. M. F. Durif, H. I. Browman, J. B. Phillips, A. B. Skiftesvik, L. A. Vøllestad, and H. H. Stockhausen, *Magnetic compass orientation in the European eel*, PLoS ONE **8**, e59212 (2013).
36. A. Cresci, C. B. Paris, C. M. F. Durif, S. Shema, R. M. Bjelland, A. B. Skiftesvik, and H. I. Browman, *Glass eels (*Anguilla anguilla*) have a magnetic compass linked to the tidal cycle*, Sci. Adv. **3**, e1602007 (2017).
37. M. Baltazar-Soares, C. Eizaguirre, *Animal navigation: the eel's magnetic guide to the Gulf stream*, Current Biology **27**, R604 (2017).
38. A. Cresci, C. M. Durif, C. B. Paris, S. D. Shema, A. B. Skiftesvik, and H. I. Browman, *Glass eels (*Anguilla anguilla*) imprint the magnetic direction of tidal currents from their juvenile estuaries*, Commun. Biol. **2**, 366 (2019).
39. T. P. Quinn, *Evidence for celestial and magnetic compass orientation in lake migrating sockeye salmon fry*, J. Comp. Physiol. **137**, 243 (1980).
40. N. F. Putman, *Inherited magnetic maps in salmon and the role of geomagnetic change*, Integr. Compar. Biol. **55**, 396 (2015).
41. L. C. Naisbett-Jones, N. F. Putman, M. M. Scanlan, D. L. G. Noakes, and K. J. Lohmann, *Magnetoreception in fishes: the effect of magnetic pulses on orientation of juvenile Pacific salmon*, J. Exp. Biology **223**, jeb222091 (2020).

42. K. Schulten, C. E. Swenberg, and A. Weller, *A biomagnetic sensory mechanism based on magnetic field modulated coherent electron spin motion*, Z. Phys. Chem. **111**, 1 (1978).
43. C. B. Grissom, *Magnetic field effects in biology: A survey of possible mechanisms with emphasis on radical-pair recombination*, Chem. Rev. **95**, 3 (1995).
44. T. Ritz, S. Adem, and K. Schulten, *A model for photoreceptor-based magnetoreception in birds*, Biophys. J. **78**, 707 (2000).
45. P. J. Hore and H. Mouritsen, *The radical-pair mechanism of magnetoreception*, Annu. Rev. Biophys. **45**, 299 (2016).
46. H. G. Hiscock, S. Worster, D. R. Kattinig, C. Steers, Y. Jina, D. E. Manolopoulos, H. Mouritsen, and P. J. Hore, *The quantum needle of the avian magnetic compass*, Proc. Natl. Acad. Sci. USA **113**, 4634 (2016).
47. S. Mann, N. H. C. Sparks, M. M. Walker, and J. L. Kirschvink, *Ultrastructure, morphology and organization of biogenic magnetite from sockeye salmon, Oncorhynchus nerka: implications for magnetoreception*, J. Exp. Biol. **140**, 35 (1998).
48. J. L. Kirschvink, M. M. Walker, and C. E. Diebel, *Magnetite-based magnetoreception*, Curr. Op. Neurobiol. **11**, 462 (2001).
49. M. Winklhofer, *Magnetite-based magnetoreception in higher organisms*, in Microbiol. Monogr., D. Schüler, *Magnetoreception and magnetosomes in bacteria* (Springer-Verlag Berlin Heidelberg 2006).
50. G. Fleissner, B. Stahl, P. Thalau, G. Falkenberg, and G. Fleissner, *A novel concept of Fe-mineral-based magnetoreception: histological and physicochemical data from the upper beak of homing pigeons*, Naturwissenschaften **94**, 631 (2007).
51. H. Cadiou and P. A. McNaughton, *Avian magnetite-based magnetoreception: a physiologist's perspective*, J. R. Soc. Interface **7**, S193 (2010).
52. A. J. Kalmijn, *Electric and Magnetic Field Detection in Elasmobranch Fishes*, Science **218**, 916 (1982).
53. B. Rosenblum, R. L. Jungerman, and L. Longfellow, *Limits to induction-based magnetoreception*, in J. L. Kirschvink, D. S. Jones, and B. J. MacFadden, B.J. (eds) *Magnetite biomineralization and magnetoreception in organisms* (Springer, Boston, 1985).
54. T. C. A. Molteno and W. L. Kennedy, *Navigation by induction-based magnetoreception in elasmobranch fishes*, J. Biophys. **2009**, 380976 (2009).
55. S. Nimpf, G. C. Nordmann, D. Kagerbauer, E. P. Malkemper, L. Landler, A. Papadaki-Anastasopoulou, L. Ushakova, A. Wenninger-Weinzierl, M. Novatchkova, P. Vincent, T. Lendl, M. Colombini, M. J. Mason, and D. A. Keays, *A putative mechanism for magnetoreception by electromagnetic induction in the pigeon inner ear*, Current Biology **29**, 4052 (2019).
56. S. Qin, H. Yin, C. Yang, Y. Dou, Z. Liu, P. Zhang, H. Yu, Y. Huang, J. Feng, J. Hao, J. Hao, L. Deng, X. Yan, X. Dong, Z. Zhao, T. Jiang, H.-W. Wang, S.-J. Luo, and C. Xie, *A magnetic protein biocompass* Nature Mater. **15**, 217 (2016).
57. D. I. Gordon and R. E. Brown, *Recent advances in fluxgate magnetometry*, IEEE Trans. Magn. **MAG8**, 76 (1972).
58. P. Ripka, *Review of fluxgate sensors*, Sens. Actuators A **33**, 129 (1992).
59. P. Ripka and M. Janošek, *Advances in Magnetic Field Sensors*, IEEE Sensors J. **10**, 1108 (2010).
60. J. P. Dowling and G. J. Milburn, *Quantum technology: the second quantum revolution*, Phil. Trans. R. Soc. Lond. A **361**, 1655 (2003).
61. I. H. Deutsch, *Harnessing the power of the second quantum revolution*, PRX Quantum **1**, 020101 (2020).
62. C. L. Degen, F. Reinhard, and P. Cappellaro, *Quantum sensing*, Rev. Mod. Phys. **89**, 035002 (2017).
63. J. Clarke, *SQUID fundamentals*, in W. H. Dordrecht, *SQUID Sensors: Fundamentals, Fabrication and Applications* (Kluwer Academic Press, 1996).
64. R. L. Fagaly, *SQUID instruments and applications*, Rev. Sci. Instr. **77**, 101101 (2006).
65. M. Schmelz, V. Zakosarenko, T. Schönau, S. Anders, S. Linzen, R. Stolz, and H.-G. Meyer, *Nearly quantum limited nanoSQUIDs based on cross-type Nb/AlO<sub>x</sub>/Nb junctions*, Supercond. Sci. Technol. **30**, 014001 (2017).
66. I. K. Kominis, T. W. Kornack, J. C. Allred, and M. V. Romalis, *A subfemtotesla multichannel atomic magnetometer*, Nature **422**, 596 (2003).
67. A. Fabricant, I. Novikova, and G. Bison, *How to build a magnetometer with thermal atomic vapor: a tutorial*, New J. Phys. **25** 025001 (2023).
68. G. Balasubramanian, I. Y. Chan, R. Kolesov, M. Al-Hmoud, J. Tisler, C. Shin, C. Kim, A. Wojcik, P. R. Hemmer, A. Krueger, T. Hanke, A. Leitenstorfer, R. Bratschitsch, F. Jelezko, and J. Wrachtrup, *Nanoscale imaging magnetometry with diamond spins under ambient conditions*, Nature **455**, 648 (2008).



69. J. M. Taylor, P. Cappellaro, L. Childress, L. Jiang, D. Budker, P. R. Hemmer, A. Yacoby, R. Walsworth, and M. D. Lukin, *High-sensitivity diamond magnetometer with nanoscale resolution*, *Nature Phys.* **4**, 810 (2008).
70. H. Zheng, Z. Sun, G. Chatzidrosos, C. Zhang, K. Nakamura, H. Sumiya, T. Ohshima, J. Isoya, J. Wrachtrup, A. Wickenbrock, and D. Budker, *Microwave-free vector magnetometry with nitrogen-vacancy centers along a single axis in diamond*, *Phys. Rev. Appl.* **13**, 044023 (2020).
71. M. Vengalattore, J. M. Higbie, S. R. Leslie, J. Guzman, L. E. Sadler, and D. M. Stamper-Kurn, *High-resolution magnetometry with a spinor bose-einstein condensate*, *Phys. Rev. Lett.* **98**, 200801 (2007).
72. P. Gomez, F. Martin, C. Mazzinghi, D. B. Orenes, S. Palacios, and M. W. Mitchell, *Bose-Einstein condensate comagnetometer*, *Phys. Rev. Lett.* **124**, 170401 (2020).
73. K. Gietka, F. Mivehvar and T. Busch, *Cavity-enhanced magnetometer with a spinor Bose-Einstein condensate*, *New J. Phys.* **23**, 043020 (2021).
74. M. Hämläinen, R. Hari, R. J. Ilmoniemi, J. Knuutila, and O. V. Lounasmaa, *Magnetoencephalography - theory, instrumentation, and applications to noninvasive studies of the working human brain*, *Rev. Mod. Phys.* **65**, 413 (1993).
75. H. Xia, A. B.-A. Baranga, D. Hoffman, and M. V. Romalis, *Magnetoencephalography with an atomic magnetometer*, *Appl. Phys. Lett.* **89**, 211104 (2006).
76. E. J. Pratt, M. Ledbetter, R. Jiménez-Martínez, B. Shapiro, A. Solon, G. Z. Iwata, S. Garber, J. Gormley, D. Decker, D. Delgadillo, A. T. Dellis, J. Phillips, G. Sundar, J. Leung, J. Coyne, M. McKinley, G. Lopez, S. Homan, L. Marsh, M. Zhang, V. Maurice, B. Siepser, T. Giovannoli, B. Leverett, G. Lerner, S. Seidman, V. DeLuna, K. Wright-Freeman, J. Kates-Harbeck, T. Lasser, H. Mohseni, T.J. Sharp, A. Zorzos, A. H. Lara, A. Kouhzadi, A. Ojeda, P. Chopra, Z. Bednarke, M. Henninger, J. K. Alford, *Kernel Flux: a whole-head 432-magnetometer optically-pumped magnetoencephalography (OP-MEG) system for brain activity imaging during natural human experiences*, *Proc. SPIE* **11700**, 1170032 (2021).
77. T. M. Tierney, N. Holmes, S. Mellor, J. D. López, G. Roberts, R. M. Hill, E. Boto, J. Leggett, V. Shah, M. J. Brookes, R. Bowtell, G. R. Barnes, *Optically pumped magnetometers: From quantum origins to multi-channel magnetoencephalography*, *NeuroImage* **199**, 598 (2019).
78. R. Zhang, W. Xiao, Y. Ding, Y. Feng, X. Peng, L. Shen, C. Sun, T. Wu, Y. Wu, Y. Yang, Z. Zheng, X. Zhang, J. Chen, and H. Guo, *Recording brain activities in unshielded Earth's field with optically pumped atomic magnetometers*, *Sci. Adv.* **6**, eaba8792 (2020).
79. G. Bison, R. Wynands, and A. Weis, *A laser-pumped magnetometer for the mapping of human cardiomagnetic fields*, *Appl. Phys. B* **76**, 325 (2003).
80. J. Kim, I. Savukov, and S. Newman, *Magnetocardiography with a 16-channel fiber-coupled single-cell Rb optically pumped magnetometer*, *Appl. Phys. Lett.* **114**, 143702 (2019).
81. M. V. Romalis and H. B. Dang, *Atomic magnetometers for materials characterization*, *Mater. Today* **14**, 258 (2011).
82. F. Fabre, A. Finco, A. Purbawati, A. Hadj-Azzem, N. Rougemaille, J. Coraux, I. Philip, and V. Jacques, *Characterization of room-temperature in-plane magnetization in thin flakes of CrTe<sub>2</sub> with a single-spin magnetometer*, *Phys. Rev. Materials* **5**, 034008 (2021).
83. N. Aslam, H. Zhou, E. K. Urbach, M. J. Turner, R. L. Walsworth, M. D. Lukin, and H. Park, *Quantum sensors for biomedical applications*, *Nature Rev. Phys.* **5**, 157 (2023).
84. B. Bao, Y. Hua, R. Wang, and D. Li, *Quantum-based magnetic field sensors for biosensing*, *Adv. Quantum Technol.* **6**, 2200146 (2023).
85. M. W. Mitchell and S. P. Alvarez, *Colloquium: Quantum limits to the energy resolution of magnetic field sensors*, *Rev. Mod. Phys.* **92**, 021001 (2020).
86. M. Meister, *Physical limits to magnetogenetics*, *eLife* **5**, e17210 (2016).
87. S. F. Huelga and M. B. Plenio, *Vibrations, quanta and biology*, *Contemp. Phys.* **54**, 181 (2013).
88. I. K. Kominis, *Quantum Zeno effect explains magnetic-sensitive radical-ion-pair reactions*, *Phys. Rev. E* **80**, 056115 (2009).
89. J. Cai, G. G. Guerreschi, and H. J. Briegel, *Quantum control and entanglement in a chemical compass*, *Phys. Rev. Lett.* **104**, 220502 (2010).
90. I. K. Kominis, *Magnetic sensitivity and entanglement dynamics of the chemical compass*, *Chem. Phys. Lett.* **542**, 143 (2012).
91. C. Y. Cai, Q. Ai, H. T. Quan, and C. P. Sun, *Sensitive chemical compass assisted by quantum criticality*, *Phys. Rev. A* **85**, 022315 (2012).



92. J. Cai and M. B. Plenio, *Chemical compass model for avian magnetoreception as a quantum coherent device*, Phys. Rev. Lett. **111**, 230503 (2013).
93. Y. Zhang, G. P. Berman, and S. Kais, *Sensitivity and entanglement in the avian chemical compass*, Phys. Rev. E **90**, 042707 (2014).
94. V. S. Poonia, K. Kondabagil, D. Saha, and S. Ganguly, *Functional window of the avian compass*, Phys. Rev. E **95**, 052417 (2017).
95. K. M. Vitalis and I. K. Kominis, *Quantum-limited biochemical magnetometers designed using the Fisher information and quantum reaction control*, Phys. Rev. A **95**, 032129 (2017).
96. M. Tolunay, I. Liepuoniute, M. Vyushkova, and B. A. Jones, Phys. Chem. Chem. Phys. **25**, 15115 (2023).
97. A. Streltsov, G. Adesso, and M. B. Plenio, *Colloquium: Quantum coherence as a resource*, Rev. Mod. Phys. **89**, 041003 (2017).
98. M. B. Plenio and S. Virmani, *An introduction to entanglement measures*, Quant. Inf. Comput. **7**, 1 (2007).
99. I. K. Kominis, *Quantum relative entropy shows singlet-triplet coherence is a resource in the radical-pair mechanism of biological magnetic sensing*, Phys. Rev. Res. **2**, 023206 (2020).
100. I. K. Kominis, *Physiological search for quantum biological sensing effects based on the Wigner-Yanase connection between coherence and uncertainty*, Adv. Quantum Technol. **2300292** (2023).
101. G. Hou, D. Wang, K. Xiao, H. Zhang, S. Zheng, P. Li, Y. Tian, and L. Jiang, *Magnetic gated biomimetic artificial nanochannels for controllable ion transportation inspired by homing pigeon*, Small **14**, 1703369 (2018).
102. Yei Hwan Jung, Byeonghak Park, Jong Uk Kim, and Tae-il Kim, *Bioinspired electronics for artificial sensory systems*, Adv. Mater. **31**, 1803637 (2019).
103. L. Xue, T. Hu, Z. Guo, C. Yang, Z. Wang, S. Qin, P. Yang, C. Xie, J. Xu, N. Li, Y. Shen, H. Jiang, D. Deng, N. Gu, and J. Sun, *A novel biomimetic magnetosensor based on magneto-optically involved conformational variation of MagR/Cry4 complex*, Adv. Electron. Mater. **1901168** (2020).
104. I. K. Kominis, *Quantum thermodynamic derivation of the energy resolution limit in magnetometry*, arXiv:2405.14687.
105. A. Vinante, C. Timberlake, D. Budker, D. F. Jackson Kimball, A. O. Sushkov, and H. Ulbricht, *Surpassing the energy resolution limit with ferromagnetic torque sensors*, Phys. Rev. Lett. **127**, 070801 (2021).
106. S. P. Alvarez, P. Gomez, S. Coop, R. Zamora-Zamora, C. Mazzinghi, and M. W. Mitchell, *Single-domain Bose condensate magnetometer achieves energy resolution per bandwidth below  $\hbar$* , Proc. Nat. Acad. USA **119**, e2115339119 (2022).
107. F. Ahrens, W. Ji, D. Budker, C. Timberlake, H. Ulbricht, and A. Vinante, *Levitated ferromagnetic magnetometer with energy resolution well below  $\hbar$* , arXiv:2401.03774.
108. I. K. Kominis, *The radical-pair mechanism as a paradigm for the emerging science of quantum biology*, Mod. Phys. Lett. B **29**, 1530013 (2015).
109. R. E. Blankenship, T. J. Schaafsma, and W. W. Parson, *Magnetic field effects on radical pair intermediates in bacterial photosynthesis*, Biochim. Biophys. Acta **461**, 297 (1977).
110. U. E. Steiner and T. Ulrich, *Magnetic field effects in chemical kinetics and related phenomena*, Chem. Rev. **89**, 51 (1989).
111. C. R. Timmel, U. Till, B. Brocklehurst, K. A. Mclauchlan, and P. J. Hore, *Effects of weak magnetic fields on free radical recombination reactions*, Mol. Phys. **95**, 71 (1998).
112. A. M. Lewis, T. P. Fay, D. E. Manolopoulos, C. Kerpel, S. Richert, and C. R. Timmel, *On the low magnetic field effect in radical pair reactions*, J. Chem. Phys. **149**, 034103 (2018).
113. S. Y. Wong, P. Benjamin, and P. J. Hore, *Magnetic field effects on radical pair reactions: estimation of  $B_{1/2}$  for flavin-tryptophan radical pairs in cryptochromes*, Phys. Chem. Chem. Phys. **25**, 975 (2023).
114. T. Ritz, R. Wiltschko, P. J. Hore, C. T. Rodgers, K. Stapput, P. Thalau, C. R. Timmel, and W. Wiltschko, *Magnetic compass of birds is based on a molecule with optimal directional sensitivity*, Biophys. J. **96**, 3451 (2009).
115. G. E. Katsoprinakis, A. T. Dellis, I. K. Kominis, *Coherent triplet excitation suppresses the heading error of the avian compass*, New J. Phys. **12**, 085016 (2010).
116. J. C. S. Lau, C. T. Rodgers, and P. J. Hore, *Compass magnetoreception in birds arising from photo-induced radical pairs in rotationally disordered cryptochromes*, J. R. Soc. Interface **9**, 3329 (2012).
117. Y. Zhang, Z. Hu, Y. Wang, and S. Kais, *Quantum simulation of the radical pair dynamics of the avian compass*, J. Phys. Chem. Lett. **14**, 832 (2023).
118. T. Ritz, P. Thalau, J. B. Phillips, R. Wiltschko, and W. Wiltschko, *Resonance effects indicate a radical-pair mechanism for avian magnetic compass*, Nature **429**, 177 (2004).

119. N. Keary, T. Ruploh, J. Voss, P. Thalau, R. Wiltschko, W. Wiltschko, and H.-J. Bischof, *Oscillating magnetic field disrupts magnetic orientation in Zebra finches, Taeniopygia guttata*, Front. Zool. **6**, 25 (2009).
120. S. Engels, N.-L. Schneider, N. Lefeldt, C. M. Hein, M. Zapka, A. Michalik, D. Elbers, A. Kittel, P. J. Hore, and H. Mouritsen, *Anthropogenic electromagnetic noise disrupts magnetic compass orientation in a migratory bird*, Nature **509**, 353 (2014).
121. B. Leberecht, D. Kobylkov, T. Karwinkel, S. Döge, L. Burnus, S. Y. Wong, S. Apte, K. Haase, I. Musielak, R. Chetverikova, G. Dautaj, M. Bassetto, M. Winklhofer, P. J. Hore, and H. Mouritsen, *Broadband 75–85 MHz radiofrequency fields disrupt magnetic compass orientation in night-migratory songbirds consistent with a flavin-based radical pair magnetoreceptor*, J. Compar. Physiol. A **208**, 97 (2022).
122. C. L. Thompson, C. B. Rickman, S. J. Shaw, J. N. Ebright, U. Kelly, A. Sancar, and D. W. Rickman, *Expression of the blue-light receptor cryptochrome in the human retina*, Invest. Ophthalmol. Vis. Sci. **44**, 4515 (2003).
123. D. Heyers, M. Manns, H. Luksch, O. Güntürkün, and H. Mouritsen, *A visual pathway links brain structures active during magnetic compass orientation in migratory birds*, PLoS One **2**, e937 (2007).
124. C. Nießner, S. Denzau, E. P. Malkemper, J. C. Gross, H. Burda, M. Winklhofer, and L. Peichl, *Cryptochrome 1 in retinal cone photoreceptors suggests a novel functional role in mammals*, Sci. Rep. **6**, 21848 (2016).
125. H. Mouritsen, U. Janssen-Bienhold, M. Liedvogel, G. Feenders, J. Stalleicken, P. Dirks, and R. Weiler, *Cryptochromes and neuronal-activity markers colocalize in the retina of migratory birds during magnetic orientation*, Proc. Natl. Acad. Sci. USA **101**, 14294 (2004).
126. J. C. Weaver, T. E. Vaughan, R. D. Astumian, *Biological sensing of small field differences by magnetically sensitive chemical reactions*, Nature **405**, 707 (2000).
127. K. Maeda, K. B. Henbest, F. Cintolesi, I. Kuprov, C. T. Rodgers, P. A. Liddell, D. Gust, C. R. Timmel, and P. J. Hore, *Chemical compass model of avian magnetoreception*, Nature **453**, 387 (2008).
128. C. Kerpel, S. Richert, J. G. Storey, S. Pillai, P. A. Liddell, D. Gust, S. R. Mackenzie, P. J. Hore, and C. R. Timmel, *Chemical compass behaviour at microtesla magnetic fields strengthens the radical pair hypothesis of avian magnetoreception*, Nat. Commun. **10**, 3707 (2019).
129. D. Budker and M. V. Romalis, *Optical magnetometry*, Nature Phys. **3**, 227 (2007).
130. S. G. Boxer, C. E. Chidsey, and M. G. Roelofs, *Anisotropic magnetic interactions in the primary radical ion-pair of photosynthetic reaction centers*, Proc. Natl. Acad. Sci. USA **79**, 4632 (1982).
131. F. Cintolesi, T. Ritz, C.W.M. Kay, C.R. Timmel, and P.J. Hore, *Anisotropic recombination of an immobilized photoinduced radical pair in a 50- $\mu$ T magnetic field: a model avian photomagnetoreceptor*, Chem. Phys. **294**, 285 (2003).
132. J. Luo, *On the anisotropic weak magnetic field effect in radical-pair reactions*, J. Chem. Phys. **158**, 234302 (2023).
133. Y. Ren, H. G. Hiscock, and P. J. Hore, *Angular precision of radical pair compass magnetoreceptors*, Biophys. J. **120**, 547 (2021).
134. A. V. Komolkin, P. Kupriyanov, A. Chudin, J. Bojarinova, K. Kavokin, and N. Chernetsov, *Theoretically possible spatial accuracy of geomagnetic maps used by migrating animals*, J. R. Soc. Interface **14**, 20161002 (2017).
135. K. J. Lohmann, K. M. Goforth, A. G. Mackiewicz, D. S. Lim, C. M. F. Lohmann, *Magnetic maps in animal navigation*, J. Compar. Physiol. A **208**, 41 (2022).
136. P. Semm and R. C. Beason, *Responses to small magnetic variations by the trigeminal system of the bobolink*, Brain Res. Bull. **25**, 735 (1990).
137. K. J. Lohmann, N. F. Putman, S. Johnsen, and C. M. F. Lohmann, *Animal magnetic sensitivity and magnetic displacement experiments*, Commun. Biol. **7**, 650 (2024).
138. I. A. Solov'yov, T. Domratcheva, A. R. M. Shahi, and K. Schulten, *Decrypting cryptochrome: revealing the molecular identity of the photoactivation reaction*, J. Am. Chem. Soc. **134**, 18046 (2012).
139. K. Maeda, A. J. Robinson, K. B. Henbest, H. J. Hogben, T. Biskup, M. Ahmad, E. Schleicher, S. Weber, C. R. Timmel, and P. J. Hore, *Magnetically sensitive light-induced reactions in cryptochrome are consistent with its proposed role as a magnetoreceptor*, Proc. Natl. Acad. Sci. USA **109**, 4774 (2012).
140. I. A. Solov'yov, T. Domratcheva, and K. Schulten, *Separation of photo-induced radical pair in cryptochrome to a functionally critical distance*, Sci. Rep. **4**, 3845 (2014).
141. D. Nohr, S. Franz, R. Rodriguez, B. Paulus, L.-O. Essen, S. Weber, and E. Schleicher, *Extended electron-transfer in animal cryptochromes mediated by a tetrad of aromatic amino acids*, Biophys. J. **111**, 301 (2016).
142. A. K. Michael, J. L. Fribourgh, R. N. Van Gelder, and C. L. Partch, *Animal cryptochromes: divergent roles in light perception, circadian timekeeping and beyond*, Photochem. Photobiol. **93**, 128 (2017).

143. D. R. Kattnig, C. Nielsen, and I. A. Solov'yov, *Molecular dynamics simulations disclose early stages of the photoactivation of cryptochrome 4*, New J. Phys. **20**, 083018 (2018).
144. B. D. Zoltowski, Y. Chelliah, A. Wickramaratne, L. Jarocho, N. Karki, W. Xu, H. Mouritsen, P. J. Hore, R. E. Hibbs, C. B. Green, and J. S. Takahashi, *Chemical and structural analysis of a photoactive vertebrate cryptochrome from pigeon*, Proc. Natl. Acad. Sci. USA **116**, 19449 (2019).
145. T. Hochstoeger, T. Al Said, D. Maestre, F. Walter, A. Vilceanu, M. Pedron, T. D. Cushion, W. Snider, S. Nimpf, G. C. Nordmann, L. Landler, N. Edelman, L. Kruppa, G. Dürnberger, K. Mechtler, S. Schuechner, E. Ogris, E. P. Malkemper, S. Weber, E. Schleicher, and D. A. Keays, *The biophysical, molecular, and anatomical landscape of pigeon CRY4: A candidate light-based quantal magnetosensor*, Sci. Adv. **6**, eabb9110 (2020).
146. G. C. G. Parico and C. L. Partch, *The tail of cryptochromes: an intrinsically disordered cog within the mammalian circadian clock*, Cell Commun. Signal. **18**, 182 (2020).
147. S. Y. Wong, Y. Wei, H. Mouritsen, I. A. Solov'yov, and P. J. Hore, *Cryptochrome magnetoreception: four tryptophans could be better than three*, J. R. Soc. Interface **18**, 20210601 (2021).
148. S. Chandrasekaran, C. M. Schneps, R. Dunleavy, C. Lin, C. C. DeOliveira, A. Ganguly, and B. R. Crane, *Tuning flavin environment to detect and control light-induced conformational switching in Drosophila cryptochrome*, Commun. Biol. **4**, 249 (2021).
149. A. Frederiksen, M. Aldag, I. A. Solov'yov, and Luca Gerhards, *Activation of cryptochrome 4 from Atlantic herring*, Biology **13**, 262 (2024).
150. J. Deviers, F. Cailliez, A. de la Lande, and D. R. Kattnig, *Avian cryptochrome 4 binds superoxide*, Comput. Struct. Biotechnol. J. **26**, 11 (2024).
151. F. Schuhmann, J. L. Ramsay, D. R. Kattnig, and I. A. Solov'yov, *Structural rearrangements of pigeon cryptochrome 4 undergoing a complete redox cycle*, J. Phys. Chem. B **128**, 3844 (2024).
152. H. Wu, A. Scholten, A. Einwich, H. Mouritsen, K. -W. Koch, *Protein-protein interaction of the putative magnetoreceptor cryptochrome 4 expressed in the avian retina*, Sci. Rep. **10**, 7364 (2020).
153. A. Günther, A. Einwich, E. Sjulstok, R. Feederle, P. Bolte, K.-W. Koch, I. A. Solov'yov, and H. Mouritsen, *Double-cone localization and seasonal expression pattern suggest a role in magnetoreception for European robin cryptochrome 4*, Curr. Biol. **28**, 211 (2018).
154. A. Pinzon-Rodriguez, S. Bensch, and R. Muheim, *Expression patterns of cryptochrome genes in avian retina suggest involvement of Cry4 in light-dependent magnetoreception*, J. R. Soc. Interface **15**, 20180058 (2018).
155. T. Biskup, E. Schleicher, A. Okafuji, G. Link, K. Hitomi, E. D. Getzoff, and S. Weber, *Direct observation of a photoinduced radical-pair intermediate in a cryptochrome DASH blue-light photoreceptor*, Angew. Chem., Int. Ed. **48**, 404 (2009).
156. D. R. Kattnig, I. A. Solov'yov and P. J. Hore, *Electron spin relaxation in cryptochrome-based magnetoreception*, Phys. Chem. Chem. Phys. **18**, 12443 (2016).
157. T. P. Fay, L. P. Lindoy, D. E. Manolopoulos, and P. J. Hore, *How quantum is radical pair magnetoreception?*, Faraday Discuss. **221**, 77 (2020).
158. S. Worster, D. R. Kattnig, and P. J. Hore, *Spin relaxation of radicals in cryptochrome and its role in avian magnetoreception*, J. Chem. Phys. **145**, 035104 (2016).
159. B. Lei, *Rod-driven OFF pathway responses in the distal retina: dark-adapted flicker electroretinogram in mouse*, PLoS ONE **7**, e43856 (2012).
160. O. Efimova and P. J. Hore, , Biophys. J. **94**, 156 (2008).
161. R. P. Blakemore, *Magnetotactic bacteria*, Ann. Rev. Microbiol. **36**, 217 (1981).
162. H. A. Lowenstam, *Minerals formed by organisms*, Science **211**, 1126 (1981).
163. D. Faivre and D. Schüler, *Magnetotactic bacteria and magnetosomes*, Chem. Rev. **108**, 4875 (2008).
164. W. Lin, J. L. Kirschvink, G. A. Paterson, D. A. Bazylinski and Y. Pan, *On the origin of microbial magnetoreception*, Natl. Sci. Rev. **7**, 472 (2020).
165. C. L. Monteil and C. T. Lefevre, *Magnetoreception in microorganisms*, Trends Microbiol. **28**, 266 (2020).
166. J. L. Gould, J. L. Kirschvink, and K. S. Deffeyes, *Bees have magnetic remanence*, Science **201**, 1026 (1978).
167. C.-H. Liang, C.-L. Chuang, J.-A. Jiang, and E.-C. Yang, *Magnetic sensing through the abdomen of the honey bee*, Sci. Rep. **6**, 23657 (2016).
168. S. H. K. Eder, H. Cadiou, A. Muhamad, P. A. McNaughton, J. L. Kirschvink, and M. Winklhofer, *Magnetic characterization of isolated candidate vertebrate magnetoreceptor cells*, Proc. Natl. Acad. Sci. USA **109**, 12022 (2012).

169. C. E. Diebel, R. Proksch, C. R. Green, P. Neilson, and M. M. Walker, *Magnetite defines a vertebrate magnetoreceptor*, *Nature* **406**, 299 (2000).
170. M. M. Walker, C. E. Diebel, C. V. Haugh, P. M. Pankhurst, J. C. Montgomery, and C. R. Green, *Structure and function of the vertebrate magnetic sense*, *Nature* **390**, 371 (1997).
171. R. C. Beason and W. J. Brennan, *Natural and induced magnetization in the bobolink, dolichonyx oryzivorus*, *J. Exp. Biol.*, **125**, 49 (1986).
172. J. L. Kirschvink and J. L. Gould, *Biogenic magnetite as a basis for magnetic field detection in animals*, *BioSystems* **13**, 181 (1981).
173. J. L. Kirschvink, *Magnetite biomineralization and geomagnetic sensitivity in higher animals: an update and recommendations for future study*, *Bioelectromagnetics* **10**, 239 (1989).
174. S. Begall, H. Burda, and E. P. Malkemper, *Magnetoreception in mammals*, *Adv. Stud. Behav.* **46**, 45 (2014).
175. G. Fleissner, B. Stahl, P. Thalau, G. Falkenberg, and G. Fleissner, *A novel concept of Fe-mineral-based magnetoreception: histological and physicochemical data from the upper beak of homing pigeons*, *Naturwissenschaften* **94**, 631 (2007).
176. G. Falkenberg, G. Fleissner, K. Schuchardt, M. Kuehbacher, P. Thalau, H. Mouritsen, D. Heyers, G. Wellenreuther, G. Fleissner, *Avian magnetoreception: elaborate iron mineral containing dendrites in the upper beak seem to be a common feature of birds*, *PLoS ONE* **5**, e9231 (2010).
177. D. Heyers, M. Zapka, M. Hoffmeister, J. M. Wild and H. Mouritsen, *Magnetic field changes activate the trigeminal brainstem complex in a migratory bird*, *Proc. Natl. Acad. Sci. USA* **107**, 9394 (2010).
178. R. Wiltschko and W. Wiltschko, *The magnetite-based receptors in the beak of birds and their role in avian navigation*, *J. Comp. Physiol. A* **199**, 89 (2013).
179. V. P. Shcherbakov and M. Winklhofer, *The osmotic magnetometer: a new model for magnetite-based magnetoreceptors in animals*, *Eur. Biophys. J.* **28**, 380 (1999).
180. G. Fleissner, G. Fleissner, B. Stahl, and G. Falkenberg, *Iron-mineral-based magnetoreception in birds: the stimulus conducting system*, *J. Ornithol.* **148**, S643 (2007).
181. I. A. Solov'yov and W. Greiner, *Theoretical analysis of an iron mineral-based magnetoreceptor model in birds*, *Biophys. J.* **93**, 1493 (2007).
182. M. Winklhofer, and J. L. Kirschvink, *A quantitative assessment of torque-transducer models for magnetoreception*, *J. R. Soc. Interface* **7**, S273 (2010).
183. A.F. Davila, G. Fleissner, M. Winklhofer, N. Petersen, *A new model for a magnetoreceptor in homing pigeons based on interacting clusters of superparamagnetic magnetite*, *Phys. Chem. Earth* **28**, 647 (2003).
184. M. Torbati, K. Mozaffari, L. Liu, and P. Sharma, *Coupling of mechanical deformation and electromagnetic fields in biological cells*, *Rev. Mod. Phys.* **94**, 025003 (2022).
185. D. T. Grob, N. Wise, O. Oduwale, and S. Sheard, *Magnetic susceptibility characterisation of superparamagnetic microspheres*, *J. Magn. Magn. Mater.* **452**, 134 (2018).
186. J. Ashmore, *Cochlear outer hair cell motility*, *Physiol. Rev.* **88**, 173 (2008).
187. P. S. Langan, V. G. Vandavasi, W. Kopec, B. Sullivan, P. V. Afonne, K. L. Weiss, B. L. de Groot, and L. Coates, (2020), *The structure of a potassium-selective ion channel reveals a hydrophobic gate regulating ion permeation*, *IUCrJ* **7**, 835 (2020).
188. V. Puerto-Belda, J. J. Ruz, C. Millá, A. Cano, M. L. Yubero, S. García, P. M. Kosaka, M. Calleja, and J. Tamayo, *Measuring vibrational modes in living human cells*, *PRX Life* **2**, 013003 (2024).
189. P. Jandačka, P. Alexa, J. Pištora, and J. Trojčková, *Hypothetical superparamagnetic magnetometer in a pigeon's upper beak probably does not work*, *Eur. Phys. J. E* **36**, 40 (2013).
190. F. Curdt, K. Haase, L. Ziegenbalg, H. Greb, D. Heyers, and M. Winklhofer, *Prussian blue technique is prone to yield false negative results in magnetoreception research*, *Sci. Rep.* **12**, 8803 (2022).
191. Z. Guo, S. Xu, X. Chen, C. Wang, P. Yang, S. Qin, C. Zhao, F. Fei, X. Zhao, P.-H. Tan, J. Wang, and C. Xie, *Modulation of MagR magnetic properties via iron-sulfur cluster binding*, *Sci. Rep.* **11**, 23941 (2021).
192. T. Tong, Y. Zhou, F. Fei, X. Zhou, Z. Guo, S. Wang, J. Zhang, P. Zhang, T. Cai, G. Li, Y. Zhang, J. Wang, and C. Xie, *The rational design of iron-sulfur cluster binding site for prolonged stability in magnetoreceptor MagR*, *Front. Mol. Biosci.* **9**, 1051943 (2022).
193. Y. Zhou, T. Tong, M. Wei, P. Zhang, F. Fei, X. Zhou, Z. Guo, J. Zhang, H. Xu, L. Zhang, S. Wang, J. Wang, T. Cai, X. Zhang, and C. Xie, *Towards magnetism in pigeon MagR: iron- and iron-sulfur binding work indispensably and synergistically*, *Zool. Res.* **44**, 142 (2023).

194. J. Zhang, Y. Chang, P. Zhang, Y. Zhang, M. Wei, C. Han, S. Wang, H.-M. Lu, T. Cai, C. Xie, *On the evolutionary trail of MagRs*, Zool. Res. **45**, 821 (2024).

**Disclaimer/Publisher's Note:** The statements, opinions and data contained in all publications are solely those of the individual author(s) and contributor(s) and not of MDPI and/or the editor(s). MDPI and/or the editor(s) disclaim responsibility for any injury to people or property resulting from any ideas, methods, instructions or products referred to in the content.